Molecular Imaging using a Targeted Magnetic Resonance Hyperpolarized Biosensor[*]

Leif Schröder[1,2], Thomas J. Lowery[1,3], Christian Hilty[1,2], David E.Wemmer[1,3], Alexander Pines[1,2]

[1]Department of Chemistry
University of California, Berkeley

[2]Materials Sciences Division, and
[3]Physical Biosciences Division
Ernest Orlando Lawrence Berkeley National Laboratory
Berkeley, CA 94720

A magnetic resonance approach is presented that enables high-sensitivity, high-contrast molecular imaging by exploiting xenon biosensors. These sensors link xenon atoms to specific biomolecular targets, coupling the high sensitivity of hyperpolarized nuclei with the specificity of biochemical interactions. We demonstrate spatial resolution of a specific target protein in vitro at micromolar concentration, with a readout scheme that reduces the required acquisition time by >3300 fold relative to direct detection. This technique uses the signal of free hyperpolarized xenon to dramatically amplify the sensor signal via chemical exchange saturation transfer (CEST). Because it is ~10,000 times more sensitive than previous CEST methods and other molecular magnetic resonance imaging techniques, it marks a critical step towards the application of xenon biosensors as selective contrast agents in biomedical applications.

Magnetic resonance imaging (MRI) is established as a powerful method for tomography of opaque biological samples (*1*). However, its application in molecular imaging (determining the spatial distribution of specific molecules of interest) has been limited due to inherent low sensitivity (*2*). Conventional MRI techniques usually detect highly abundant nuclei, such as protons (^{1}H) of water (110 M ^{1}H concentration) and/or fat to guarantee sufficient signal intensity despite the low thermal polarization. Contrast agents, including some that bind to specific biomolecular targets, have been developed that induce small but detectable changes in these strong signals. However, the required contrast agent concentration is ~0.5 to 2 mM for signal changes based on relaxation enhancements (*2*) or saturation transfer experiments (*3*). Application of exogenous ^{129}Xe circumvents limitations in sensitivity and contrast because Xe nuclei can be hyperpolarized prior to transfer into the system of interest and their nuclear magnetic resonance (NMR) frequencies are extremely sensitive to the molecular environment. Hyperpolarization

amplifies the available magnetization by a factor of $>10^4$ and it is currently used to increase anatomical contrast in MRI for imaging of void spaces such as the lung (4).

Detection of specific biomolecules in a solution environment can be accomplished by xenon biosensors, which trap Xe atoms in molecular cages that have been functionalized to bind the desired target (5,6). Xenon biosensors are composed of a cryptophane-A cage (7), linker, and targeting moiety (Fig. 1a), which can be an antibody or ligand that enables detection of a specific analyte. The cage-encapsulated xenon nuclei give rise to a unique signal that differs significantly from that of free Xe. Hence, these compounds act as selective imaging contrast agents for near-zero background MRI that benefit from the high specificity of biochemical targeting (5,6). The excellent resolution of free and biosensor-bound Xe was used recently to obtain a one-dimensional NMR profile from a bead-immobilized biosensor in a perfusion phantom that delivers Xe saturated water to a test volume inside the NMR probe (8). This setup mimics in principle Xe delivery to a biosensor-labeled volume of interest as it would be provided by the blood stream in vivo after injection or inhalation. Direct application of the xenon biosensor to molecular imaging has been impaired by the fact that for typical experiments, only ~1% of dissolved Xe is associated with the sensor (9). A further challenge was shown to lie in the broadening of sensor signal in heterogeneous samples (8,9), leading to a significant reduction in signal-to-noise.

Here, we introduce a different approach for obtaining MR images of Xe biosensors that is based on chemical exchange between the biosensor-encapsulated Xe and the easily detectable pool of free Xe (10), thus making optimized use of the available biosensor-associated magnetization. These Xe nuclei fulfill the conditions of slow exchange on the NMR timescale, i.e., the frequency difference of the resonances ($\Delta\omega$) is large compared to the exchange rate (τ_{ex}^{-1}) between the two sites: $\Delta\omega \gg \tau_{ex}^{-1}$. Such exchange is used for

signal amplification by measuring a decrease in the intense free xenon signal after selective saturation of the biosensor-bound xenon. Exchange-mediated depletion of the free xenon signal requires that the exchange rate be fast compared to the longitudinal relaxation time of free xenon ($\tau_{ex}^{-1} \gg T_1^{-1}$) and that the saturation be effective (transition rate $W \geq \tau_{ex}^{-1}$). With a value of $T_1 \approx 66$ s in water (*11*) at 9.4 T and exchange dynamics characterized by $\tau_{ex} \approx 40$ ms (*10*), Xe nuclei in the sensor cages are ideal for saturation transfer.

The applied technique is similar to chemical exchange saturation transfer, or CEST (*12*), which was previously developed for use with proton contrast agents. However, because the method presented here, HYPER-CEST, uses hyperpolarized nuclei with a long relaxation time, nearly the entire sensor-related magnetization depletion is stored in the observed signal

This scheme allows significant sensitivity improvement, which we demonstrate with two-dimensional images that were obtained in a few minutes of a biosensor solution sample with ~5 µM concentration of a recently described biosensor construct (*8,9*) that binds via its biotin moiety to avidin-functionalized agarose beads in an aqueous environment. [129]Xe NMR spectra of such bead samples are comprised of three different signals (Fig. 1a): free Xe in the bead medium resonates at $\delta_1 = 193.6$ ppm (referred to as "bead signal" in the following), free Xe in pure water at $\delta_2 = 192.5$ ppm, and Xe inside the biosensor cage at $\delta_3 = 65.4$ ppm (chemical shifts are calibrated relative to the Xe gas signal at $\delta = 0$ ppm). Selective presaturation around δ_3 initiates the HYPER-CEST process (Fig. 1b) that accumulates selectively depolarized nuclei in a cyclic process (Fig. 1b). Because the depolarized magnetization $M_z = 0$ cannot be detected directly, the difference of MRI datasets with on- and off-resonant presaturation allows for sensitive detection of sample regions of dilute biosensor.

Chemical shift imaging (CSI) is an MRI method that preserves the intrinsic frequency information of NMR signals (*13*). It uses pulsed magnetic field gradients to generate phase encoded signals in the frequency domain and provides maps of spatially resolved NMR spectra after 2-dimensional Fourier transformation (FT). This method yields selective images for any spectral component. To demonstrate specificity of the biosensor imaging method, agarose beads were embedded in a flow system described previously *(8)* such that the volume of interest is divided into two compartments (Fig. 2a). Volume ② contained avidin-agarose beads (*9*) with biosensor bound at a concentration of 5 µM and volume ① contained biosensor-free beads. The phantom was attached to an apparatus that provides perfusion with Xe saturated water, as previously described (*8*). The concentration of detectable nuclei is equivalent to ~2 µM of 100% polarized xenon (~260 µM xenon with the natural 25% ^{129}Xe, polarized to $P = 3\%$). Direct detection of the sensor at a concentration of 50 µM in volume ② requires signal averaging of 256 transients (S/N ~ 3.5, biosensor linewidth ~210 Hz, Fig 1a), therefore ~25,000 transients are necessary to directly observe the sensor at 5 µM even without any spatial resolution. Application of the sensitive HYPER-CEST technique enables localized detection of this biosensor concentration with only two complete CSI acquisitions (SOM).

The excellent biosensor specificity is shown in Fig. 2b. A reference spectrum is given for off-resonant 4 s continuous wave (cw) saturation at $\delta_{off} = \delta_1 + (\delta_1 - \delta_3) = \delta_1 + \Delta$. Switching the frequency to $\delta_{on} = \delta_1 - \Delta = \delta_3$ causes a significant depletion of the bead signal at δ_1 for ②, whereas the spectrum from volume ① remains essentially unaffected. Hence, the Fourier transform of the difference raw data only contains bead signal for areas participating in the saturation transfer as a consequence of biosensor labeling.

The corresponding images given in Fig. 3 illustrate the inherent multimodal contrast of our technique, i.e. imaging contrast provided by both the chemical shift information and

the tunable HYPER-CEST effect. The dataset with off-resonant presaturation displays the compartments that contain both types of beads when only the signal intensity at δ_1 is evaluated (Fig. 3a). This Xe image matches precisely the geometry seen in the conventional ^{1}H MR image in Fig. 2a. Additional information is given by plotting the signal distribution of the solution dissolved xenon peak, δ_2. It displays the surrounding outlet tube of the phantom (Fig. 3b), *i.e.*, a volume that contains the perfusion agent but that does not contain the biosensor or its molecular target. These images show a near-zero background due to the good spectral discrimination of the signal components. On-resonant presaturation depletes the δ_1 signal in compartment ②, leaving the signal in compartment ① undisturbed (Fig. 3c). The difference image for δ_1 shown in Fig. 3d only contains signal from volume ② where the biosensor is present. The solution signal remains virtually unaffected by switching the saturation frequency.

HYPER-CEST does not compete with relaxation of thermally polarized nuclei, i. e. there is no counteracting effect of re-polarization as it would be the case for the saturation of thermally polarized nuclei. Thus, the concentration of the detected nuclei can be even lower than that of the contrast agent, *i.e.* 2 µM vs. 5 µM in our case; comparison with conventional CEST applications shows the gain provided by the process of selective depletion. Using water protons as the detectable pool in conventional CEST requires large magnetic fields to decrease relaxation effects and increase the frequency difference to the saturated component. The latter problem was partially circumvented by incorporating paramagnetic ions in contrast agents, a technique called PARACEST (*3*). Because those agents have only one coordination site for water molecules, even relatively high concentrations (2mM, *i.e.* 800 times more active sites than in this study) cause a signal decrease of no more than 4 to 12%, even when the concentration of polarized nuclei is 2600 fold higher (5.2 mM for water at 7 T) compared to our setup. A contrast comparable

to the results reported here, *i.e.* a signal decrease of 40 to 50%, was observed with CEST using exchangeable sites on macromolecules at 100 μM (*14*). However, those results for poly-L-lysine were based on concentrations of 700 mM for the exchangeable sites and 8.7 mM for the polarized nuclei (water at 11.7 T). Hence, the sensitivity gain given by HYPER-CEST provides the same contrast with only 1/140,000 of active sites and 1/4350 of detectable nuclei.

The results presented emphasize the high potential for molecular imaging based on the Xe biosensor in combination with HYPER-CEST. If the same images were acquired using a conventional direct detection methodology, over 870 hrs would be required (see SOM). Therefore this technique marks a critical step towards the application of xenon biosensors as a selective contrast agent in biomedical MRI. Because the specificity of the sensor is determined by the functionality of its targeting agent, we envision that the combination of HYPER-CEST with the xenon biosensor can be used to image any molecular target for which an affinity agent (*e.g.*, ligand, antibody, etc.) is known. Sensitivity relies predominantly on the signal-to-noise ratio (SNR) of the resonance of free Xe and is independent of the biosensor signal linewidth that previously limited the SNR (*8*). Moreover, this technique provides an adjustable contrast that can be switched on and off at-will because the HYPER-CEST effect depends on the saturation power (of course, the signal contrast as given in Fig. 2b also depends on the biosensor concentration; see SOM). At this stage, we can detect a voxel of 22.5μL $\approx$ (2.8 mm)^3 in a coil volume of ca. 2.8 mL for a biosensor concentration of 5 μM. However, several possibilities for improvement should lead to even further sensitivity enhancement. Using isotopically-enriched ^{129}Xe will increase the S/N by a factor of ~4, and optimized polarization procedures (*15*) can increase the signal by another factor of 15. Hence, these straightforward optimizations decrease the limit of detection by 60-fold to ~85 nM Xe

biosensor. This limit can be further decreased by increasing the cage-to-target ratio via chemical means, by designing the probe constructs such that the target molecule binds more than one biosensor (avidin, *e.g.*, has a capacity of 4), or constructing each biosensor from more than one cryptophane cage, for example through dendrimeric amplification (*16*). Using these means the minimum concentration of the target structure should reach the low nM to high pM range for optimized *in vitro* experiments. Hence, application of HYPER-CEST to xenon biosensors represents a new dimension of sensitivity and specificity for molecular imaging. The depletion process generating the image contrast depends on several parameters, including saturation power and time, sensor concentration and ambient temperature. The latter parameter provides another promising approach to even further increase sensitivity because the exchange rate increases significantly when approaching 37°C (*10*). Characterization of the saturation dynamics is currently underway and will reveal optimized parameters for future applications.

The technique is also quite promising for biomedical imaging *in vivo*. A typical surface coil of 20 cm diameter detects a volume of ca. 2.1 L, thus decreasing SNR for a $(2.8 \text{ mm})^3$ voxel by factor 27.2 compared to our setup. This loss is less than 50% of the gain for an optimized system using >45% polarized isotopically enriched ^{129}Xe. An isotropic resolution of 2 to 3 mm is feasible without signal averaging for a concentration of pure polarized ^{129}Xe that is ~2 μM in tissue. This minimum value is below that observed for direct injection of Xe-carrying lipid solutions into rat muscle (70 μM) or that for inhalation delivery for brain tissue (8 μM) used in previous studies that demonstrated Xe tissue imaging in vivo (*17*). Sensitive molecular imaging of the biosensor is therefore possible as long as the distribution of dissolved xenon can be imaged with sufficient SNR and the biosensor target is not too dilute, because HYPER-CEST is based on the detection of the free Xe resonance, not direct detection of the biosensor resonance.

The HYPER-CEST technique is amenable to any type of MRI image acquisition methodology. We demonstrated CSI here but faster acquisition techniques that incorporate a frequency encoding domain such as FLASH have been successfully used to acquire *in vivo* Xe tissue images (*17*).

The modular set-up of the biosensor (*i.e.*, the nuclei that are detected are not covalently bound to the targeting molecule) allows accumulation of the biosensor in the tissue for minutes to hours prior to delivery of the hyperpolarized xenon nuclei which have much higher diffusivity. In combination with the long spin-lattice relaxation time of Xe, this two-step process optimally preserves the hyperpolarization before signal acquisition. Biosensor cages that yield distinct xenon frequencies allow for multiplexing to detect simultaneously several different targets (*18*). Also the serum- and tissue-specific Xe NMR signals (*19,20*) arising after injection of the carrier medium can be used for perfusion studies (see Fig. 3b) in living tissue, making Xe-CSI a multi-modal imaging technique.

REFERENCES

1. Tyszka, J. M., Fraser, S. E. & Jacobs, R. E. *Curr. Opin. Biotechnol.* **16**, 93-99 (2005).

2. Louie, A.Y. *et al. Nature Biotech.* **18**, 321-324 (2000).

3. Aime S., Carrera C., Delli Castelli D., Geninatti S., Terreno E. *Angew. Chemie Int. Ed.* **44**, 1813-1815 (2005).

4. Albert, A. S. *et al. Nature* **370**, 199-201 (1994).

5. Spence, M. M. *et al. Proc. Natl. Acad. Sci. USA* **98**, 10654-10657 (2001).

6. Lowery, T. J., *et al. Magn. Reson. Imaging.* **21**, 1235-1239 (2003).

7. Bartik, K., Luhmer, M., Dutasta, J. P., Collet, A. & Reisse, J. *J. Am. Chem. Soc.* **120**, 784-791, (1998).

8. Hilty, C., Lowery, T. J., Wemmer, D. E. & Pines, A. *Angew. Chem. Int. Ed.* **45**, 70-73 (2006).

9. Han, S.-I. *et al. Anal. Chem.* **77**, 4008-4012 (2005).

10. Spence, M. M. *et al.. J. Am. Chem. Soc.* **126**, 15287-15294 (2004).

11. Bifone, A. *et al. Proc. Natl. Acad. Sci. USA* **93**, 12932-12936 (1996).

12. Ward, K. M., Aletras, A. H. & Balaban, R. S. *J. Magn. Res.* **143**, 79-87 (2000).

13. Maudsley, A. A., Hilal, S. K., Perman, W. H. & Simon, H. E. *J. Magn. Res.* **51**, 147-152 (1983).

14. Goffeney N., Bulte J. W. M., Duyn J., Bryant L. H., van Zijl P. C. M. *J. Am. Chem. Soc* **123**, 8628-8629 (2001).

15. Knagge, K., Prange, J. & Raftery, D. *Chem. Phys. Lett.* **397**, 11-16 (2004).

16. Mynar, J. L., Lowery, T. J., Wemmer, D. E., Pines, A., Frechet, J. M. *J. Amer. Chem. Soc.* **128**, 6239-6246 (2006) .

17. Goodson, B. M. *et al. Proc. Natl. Acad. Sci. USA* **94**, 14725-14729 (1997).

18. Huber, G. *et al. J. Amer. Chem. Soc.* **128**, 6334-6335 (2006),

19. Mugler J. P., *et al. Magn. Res. Med.* **37**, 809 - 815 (1997).

20. Swanson, S. D., Rosen, M. S., Coulter, K. P., Welsh, R. C. & Chupp, T. E. *Magn. Res. Med.* **42**, 1137 - 1145 (1999).

FIGURE CAPTIONS

Fig. 1: Sensitivity-enhanced NMR detection of Xe biosensors. a) Chemical structure of the Xe biosensor illustrating the cryptophane-A cage (green), the linker (black), the targeting moiety (biotin in this case; orange), and the peptide chain (purple) that is required for sufficient water solubility. The ^{129}Xe NMR spectrum of this construct at 50 μM bound to avidin agarose beads yields only a broad, weak resonance from encapsulated Xe at δ_3, even for 256 acquisitions. Chemical exchange with free Xe outside the cage (resonance δ_1) enables sensitivity enhancement by depolarizing the δ_3 nuclei and detecting at δ_1. b) Amplifying the cage-related magnetization using HYPER-CEST. Selective saturation of biosensor-encapsulated Xe (green) and subsequent chemical exchange with the free Xe (blue) allows accumulation of depolarized nuclei (red). This procedure corresponds to continuous depolarization of cage-related magnetization that can be measured indirectly after several cycles by the difference between the initial and final bulk magnetization.

Fig. 2: Demonstration of HYPER-CEST on a two-compartment phantom. a) Transverse ^{1}H NMR image of the two-compartment phantom containing avidin-agarose beads. The biosensor is only present in volume ②. Two voxels were selected to allow demonstration of saturation transfer: the red voxel as part of the sensor-marked volume, the blue voxel as part of the control compartment. b) Localized ^{129}Xe NMR spectra (absolute signal) from the two voxels marked in a). Undisturbed resonances from the bead-associated Xe in the biosensor-labeled volume (red) and the control volume (blue) are obtained for off-resonant cw saturation whereas on-resonant saturation depletes the signal in compartment ②. The difference spectrum reveals signal only for resonances arising from species involved in the chemical exchange with the biosensor cage.

Fig. 3: Molecular imaging of the Xe biosensor (overlay of transverse ^{129}Xe images obtained from CSI datasets with the ^{1}H image shown in Fig. 2a). a) Selective image for the bead signal at δ_1 and off-resonant cw saturation. b) Selective image of the pure solution signal at δ_2. This signal clearly corresponds to the surrounding outlet tube and is not affected by any saturation transfer. c) On-resonant saturation of the biosensor resonance significantly depletes the δ_1 signal in volume ②. d) The difference image of the two CSI datasets yields an exclusive mapping of compartment ②, *i.e.*, a molecular image of the Xe biosensor.
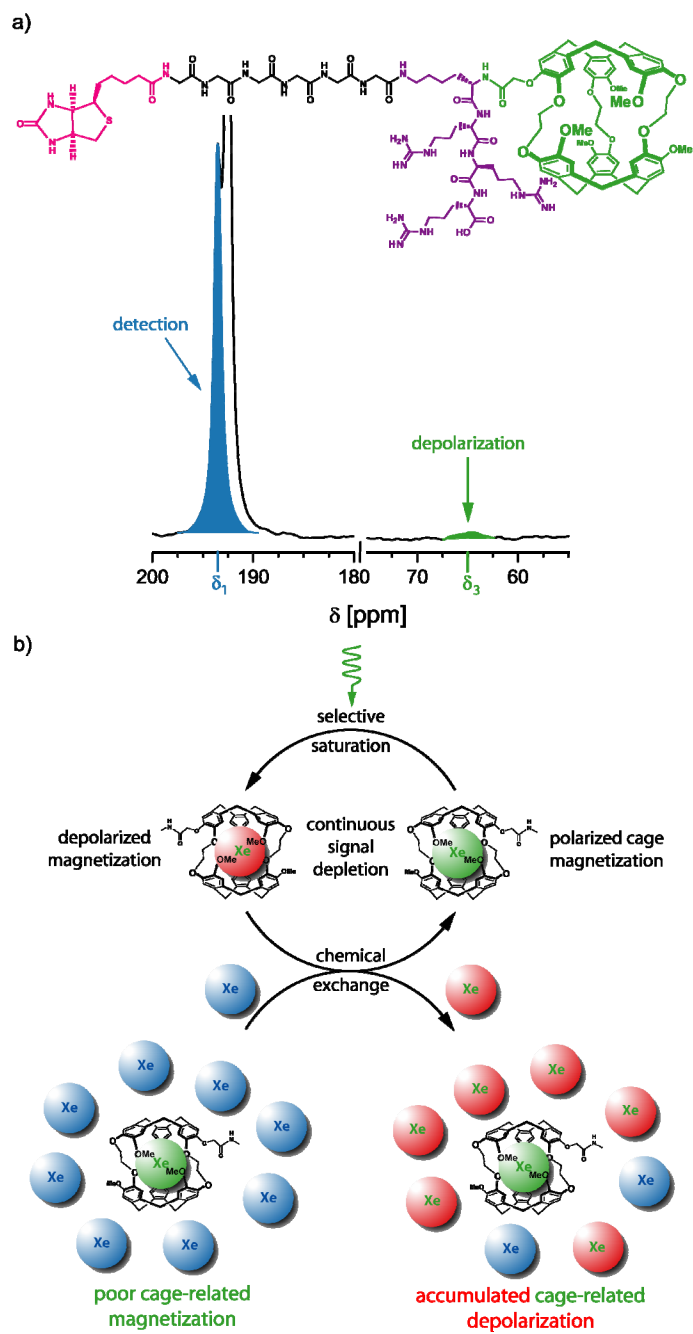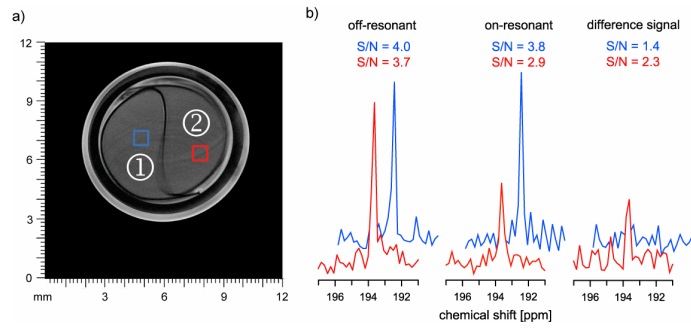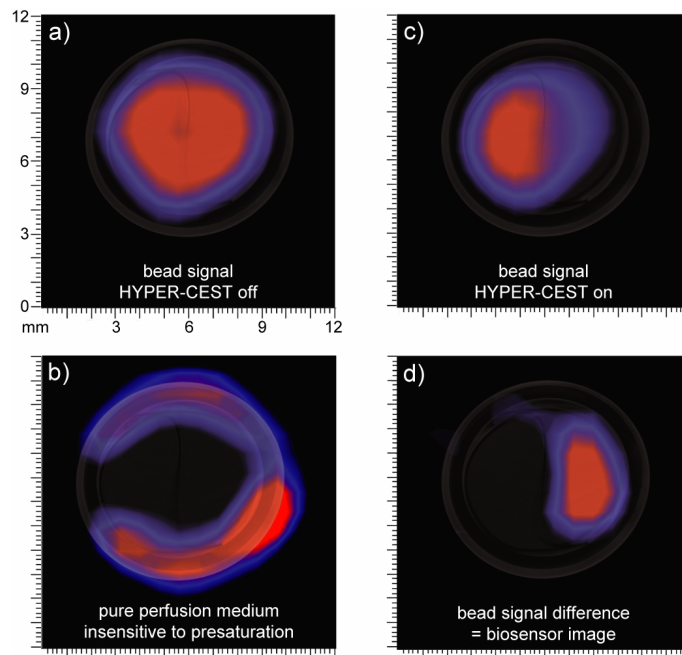
Figure 1

Figure 2

7Fig. 3:

Suggestion for Cover Illustration:

Targeted Molecular Imaging using Selective Depolarization of Hyperpolarized Xenon